Energy Materials

Supplementary Materials

Interfacial coordination reconstruction via electrochemical phase transformation for stable zinc powder anodes

Can Huang[1,#], Yuan Li[2,#], Penghui Cao[1,3,4,*], Xinqi Yang[1], Shimin Yao[1], Huali Zhu[1], Juan Yang[5], Chuanchang Li[1,3,4], Xiongjun Liu[2,*], Zhaoping Lu[2,*]

[1]Key Laboratory of Renewable Energy Electric-Technology of Hunan Province, College of Energy and Power Engineering, Changsha University of Science and Technology, Changsha 410114, Hunan, China.

[2]State Key Laboratory for Advanced Metals and Materials, University of Science and Technology Beijing, Beijing 100083, China.

[3]State Key Laboratory of Disaster Prevention & Reduction for Power Grid, Changsha University of Science & Technology, Changsha 410114, Hunan, China.

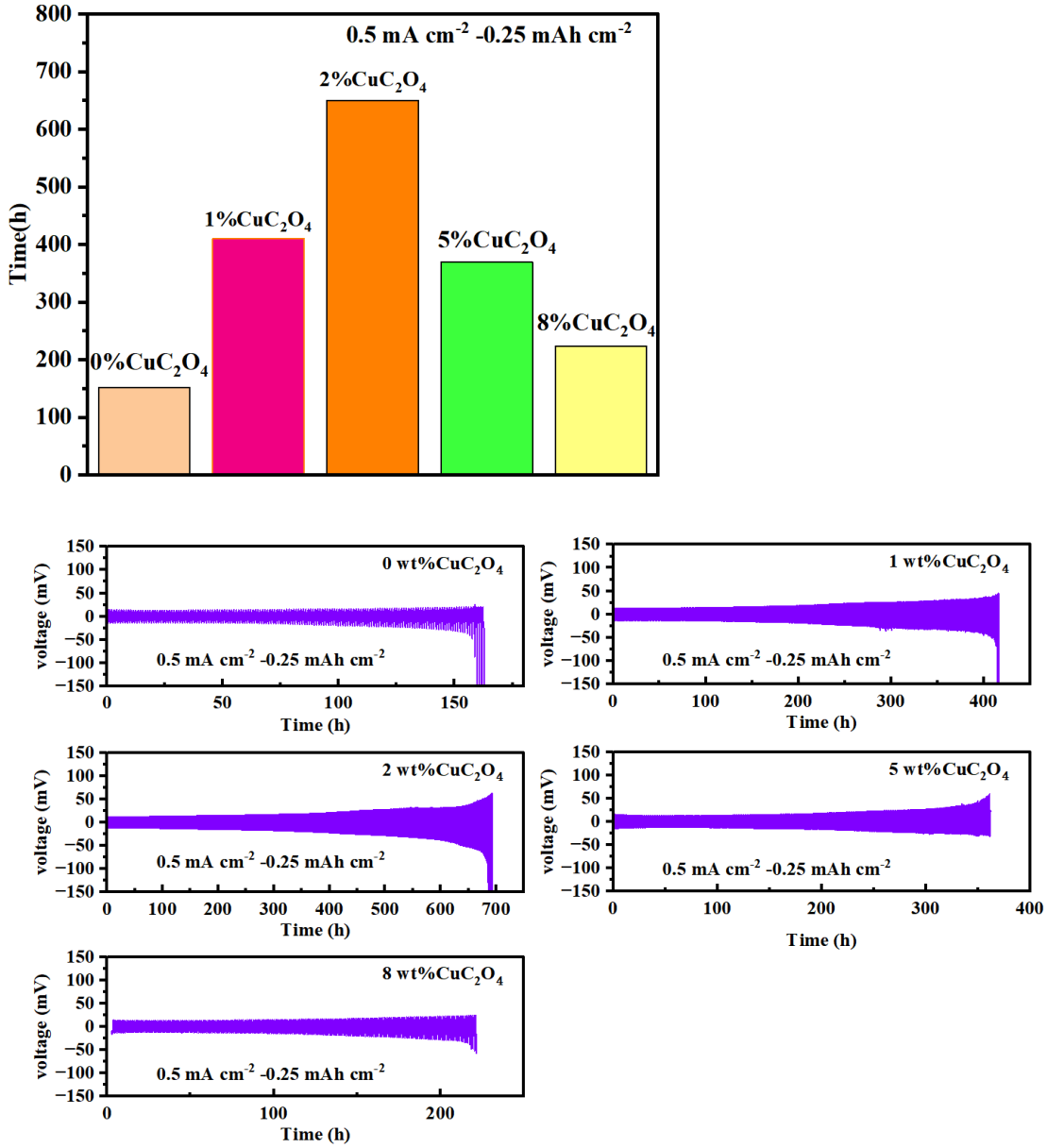
[4]Turpan Solar Thermal Resource Development and Utilization Expert Workstation, Changsha University of Science and Technology, Turpan 838000, Xinjiang, China.

[5]School of Metallurgy and Environment, Central South University, Changsha 410083, Hunan, China.

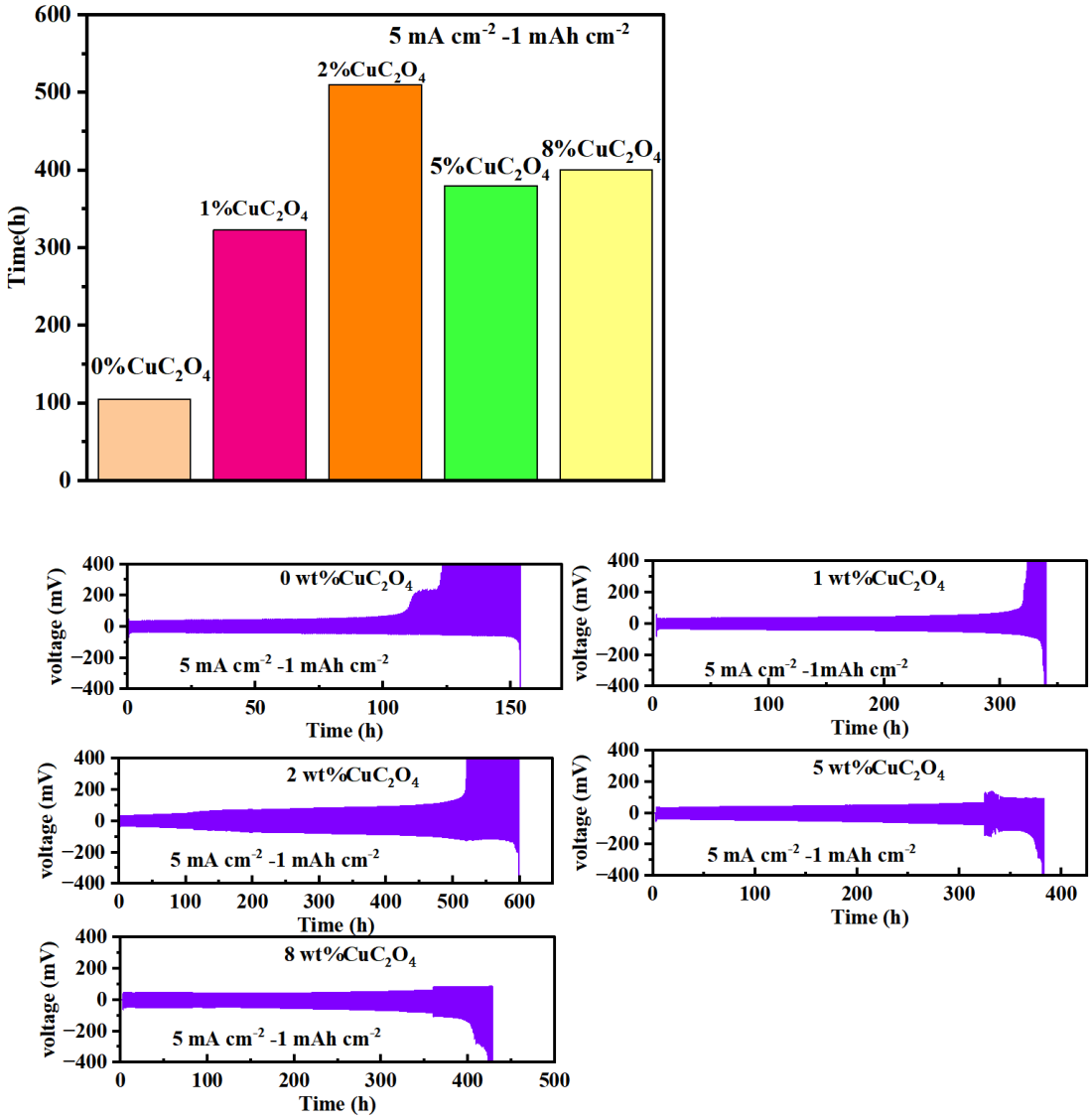
[#]These authors contributed equally to this work.

[*]**Correspondence to:** Prof. Penghui Cao, Key Laboratory of Renewable Energy Electric-Technology of Hunan Province, College of Energy and Power Engineering, Changsha University of Science and Technology, Changsha 410114, Hunan, China; State Key Laboratory of Disaster Prevention & Reduction for Power Grid, Changsha University of Science & Technology, Changsha 410114, Hunan, China; Turpan Solar Thermal Resource Development and Utilization Expert Workstation, Changsha University of Science and Technology, Turpan 838000, Xinjiang, China. E-mail: CaoPH@csust.edu.cn; Prof. Xiongjun Liu, Prof. Zhaoping Lu, State Key Laboratory for Advanced Metals and Materials, University of Science and Technology Beijing,

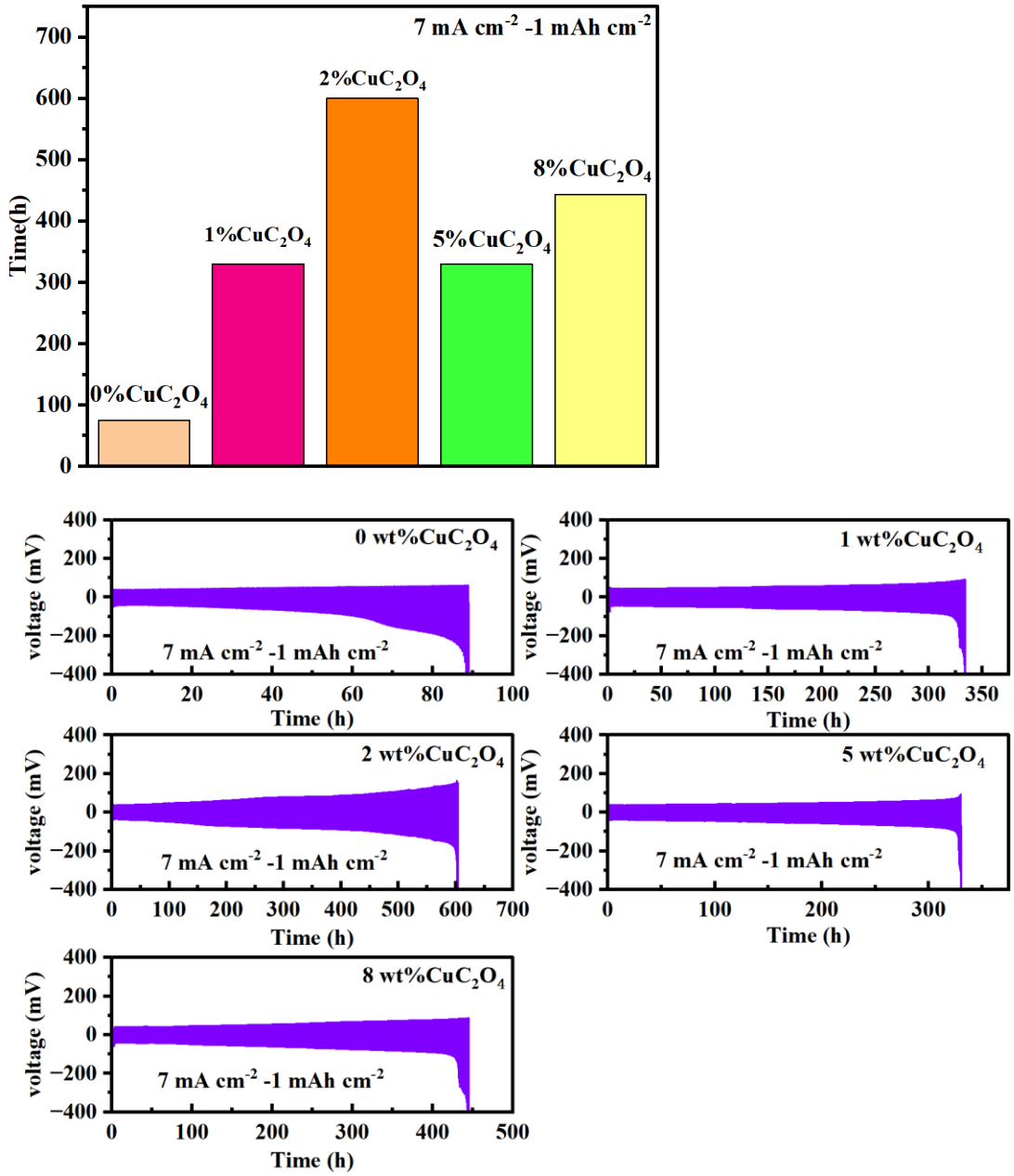
Beijing 100083, China. E-mail: xjliu@ustb.edu.cn; luzp@ustb.edu.cn



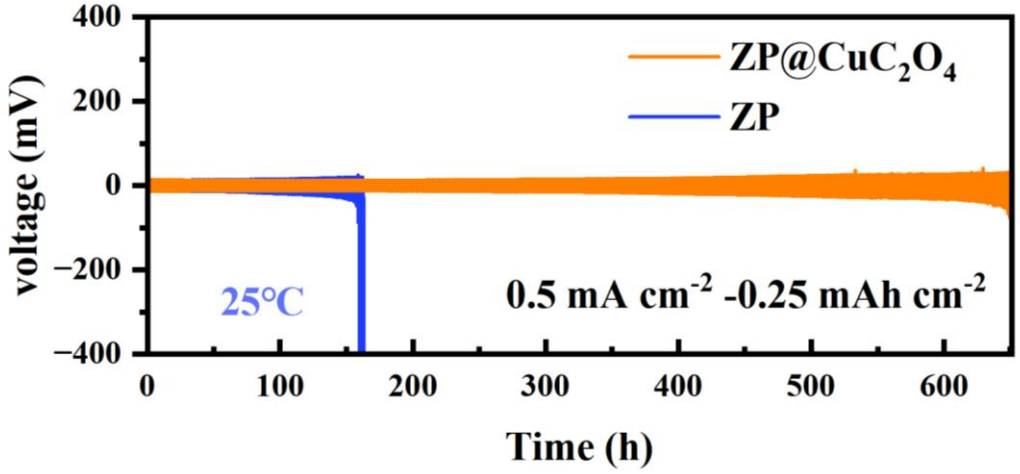
Supplementary Figure 1. Cycling stability and lifetime summary of Zn//Zn symmetric cells with different wt% CuC_2O_4 contents at 0.5 mA cm^{-2} and 0.25 mAh cm^{-2}.



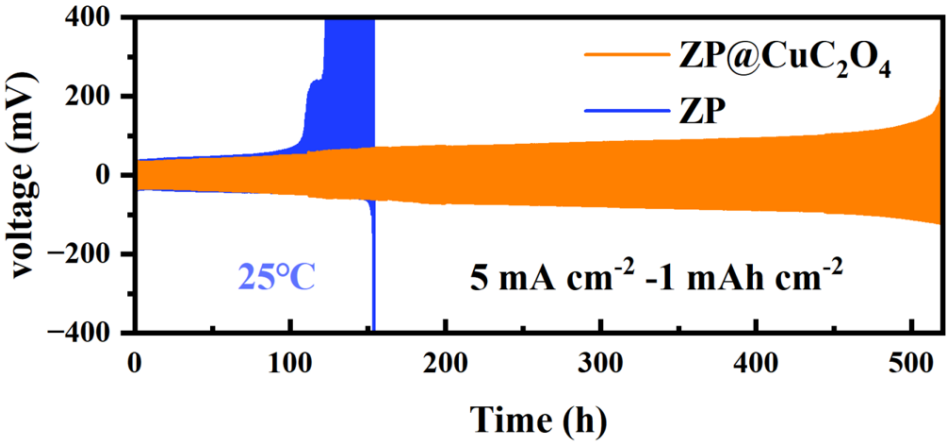
Supplementary Figure 2. Cycling stability and lifetime summary of Zn//Zn symmetric cells with different wt% CuC_2O_4 contents at 5 mA cm^{-2} and 1 mAh cm^{-2}.



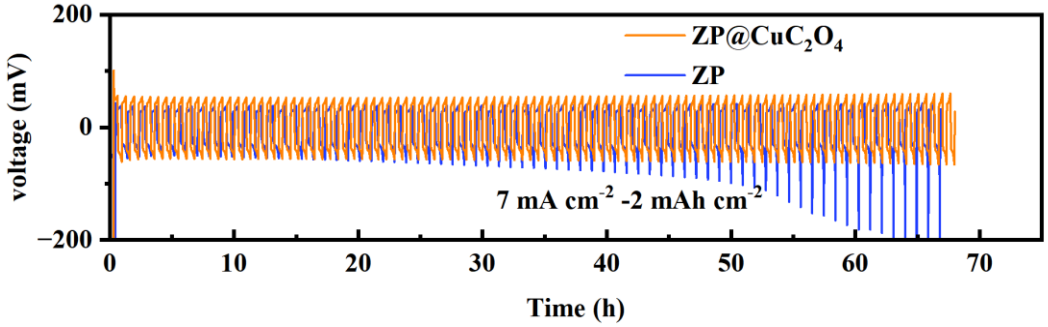
Supplementary Figure 3. Cycling stability and lifetime summary of Zn//Zn symmetric cells with different wt% CuC_2O_4 contents at 7 mA cm^{-2} and 1 mAh cm^{-2}.



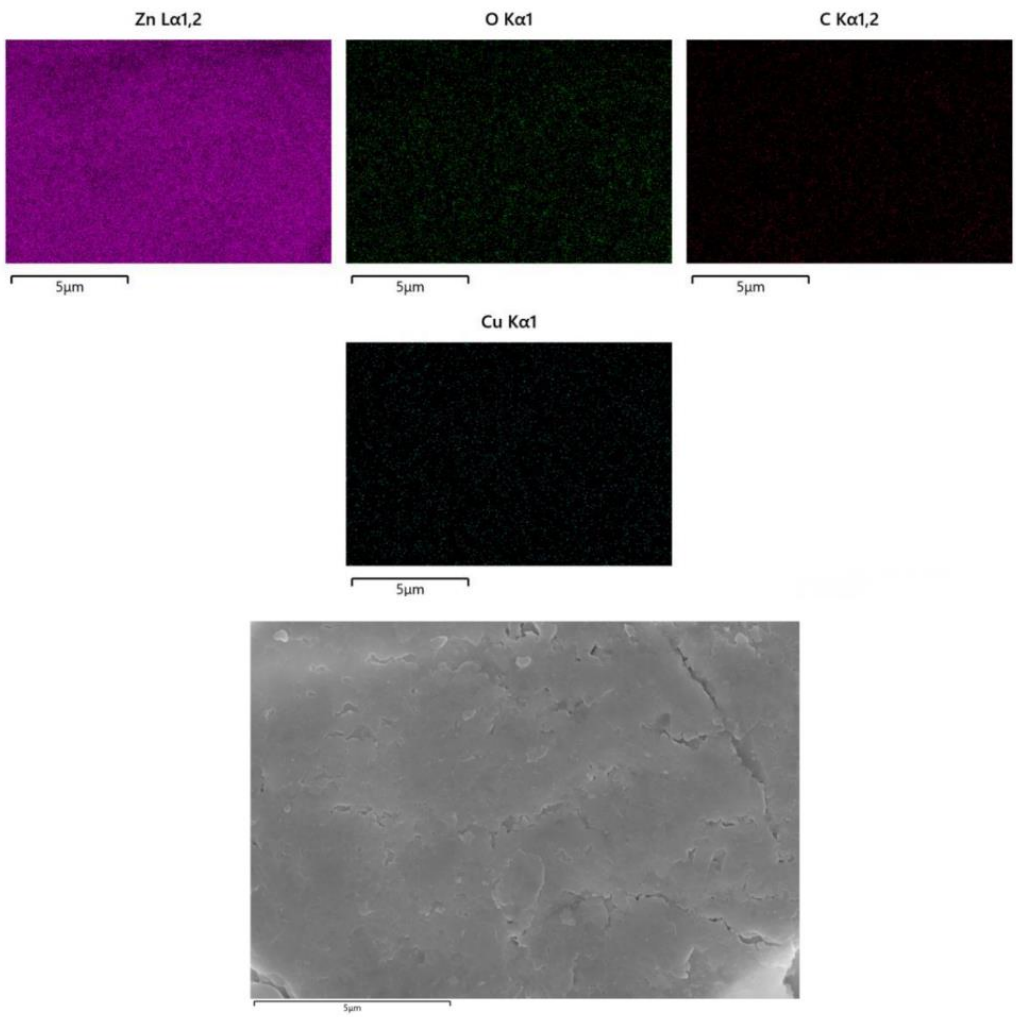
Supplementary Figure 4. Galvanostatic cycling comparison of ZP and ZP@CuC_2O_4 symmetric cells at 25 °C under 0.5 mA cm^{-2} and 0.25 mAh cm^{-2}.



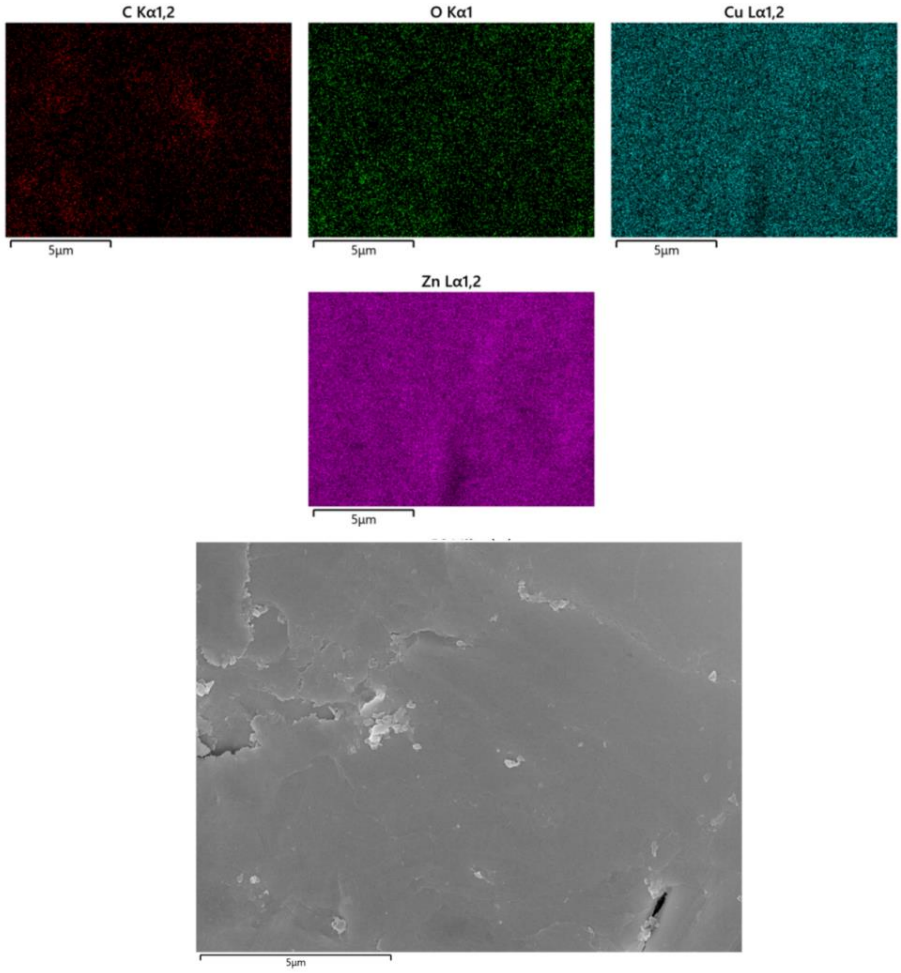
Supplementary Figure 5. Galvanostatic cycling comparison of ZP and ZP@CuC_2O_4 symmetric cells at 25 °C under 5 mA cm^{-2} and 1 mAh cm^{-2}.



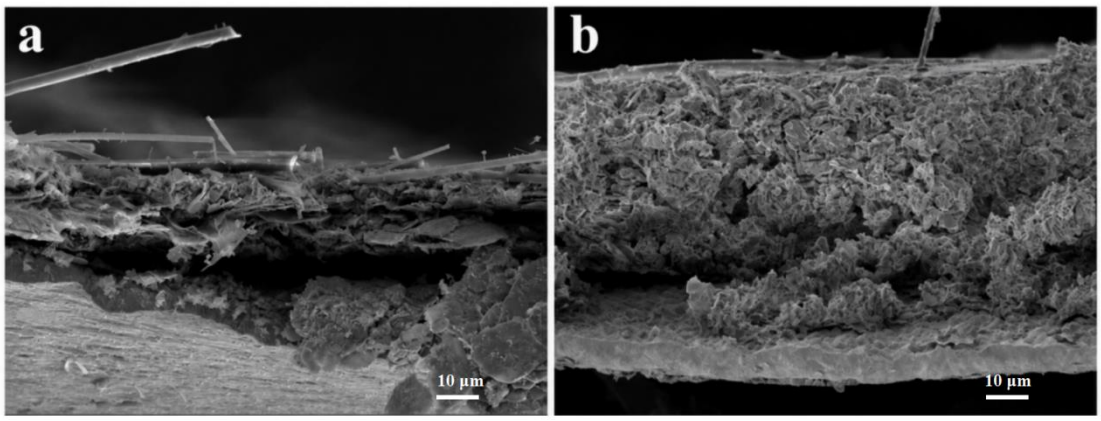
Supplementary Figure 6. Deep-discharge cycling performance of Zn symmetric cells using ZP and ZP@CuC_2O_4 electrodes at a high current density of 7 mA cm^{-2} with an areal capacity of 2 mAh cm^{-2}.



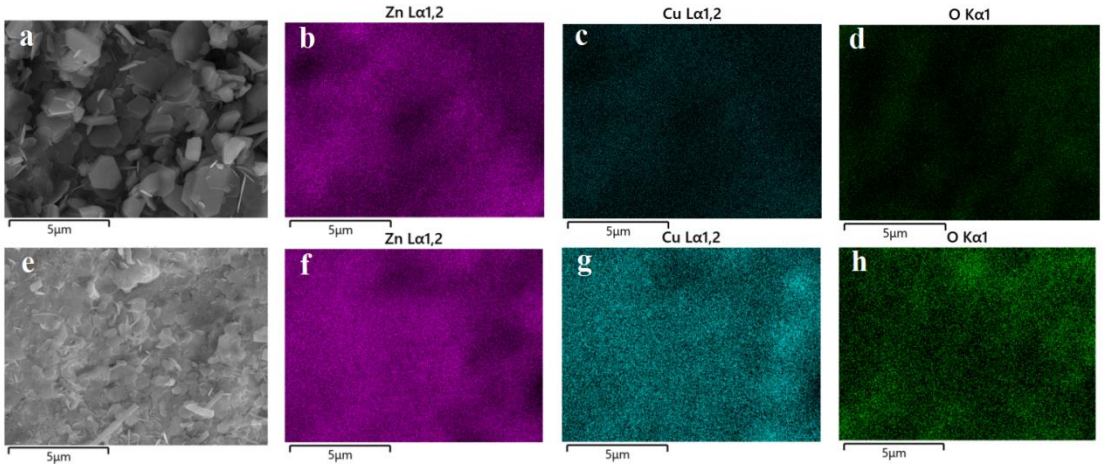
Supplementary Figure 7. SEM image and corresponding EDS elemental mapping of the pristine ZP electrode before cycling.



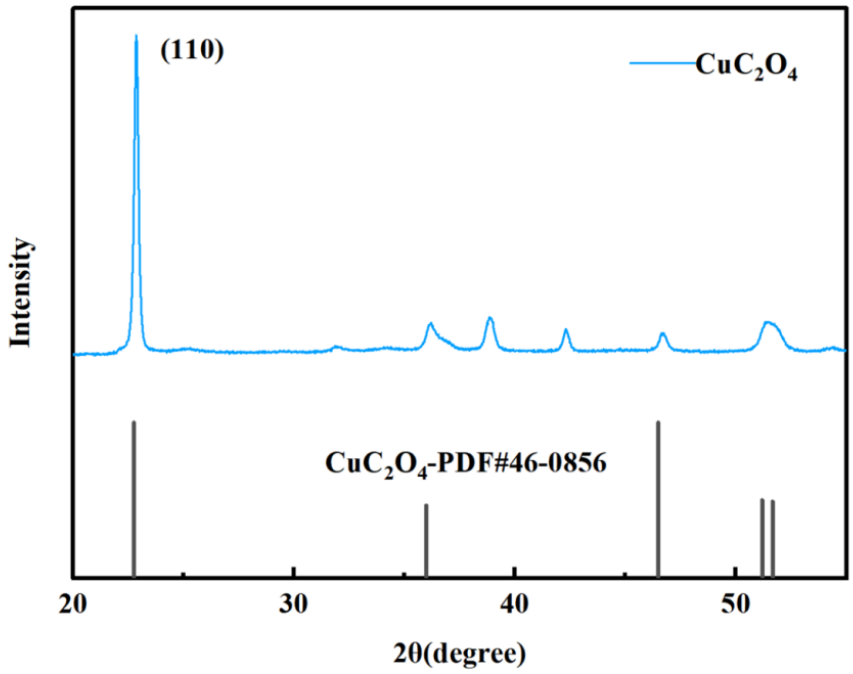
Supplementary Figure 8. SEM image and corresponding EDS elemental mapping of the pristine ZP@CuC_2O_4 electrode before cycling.



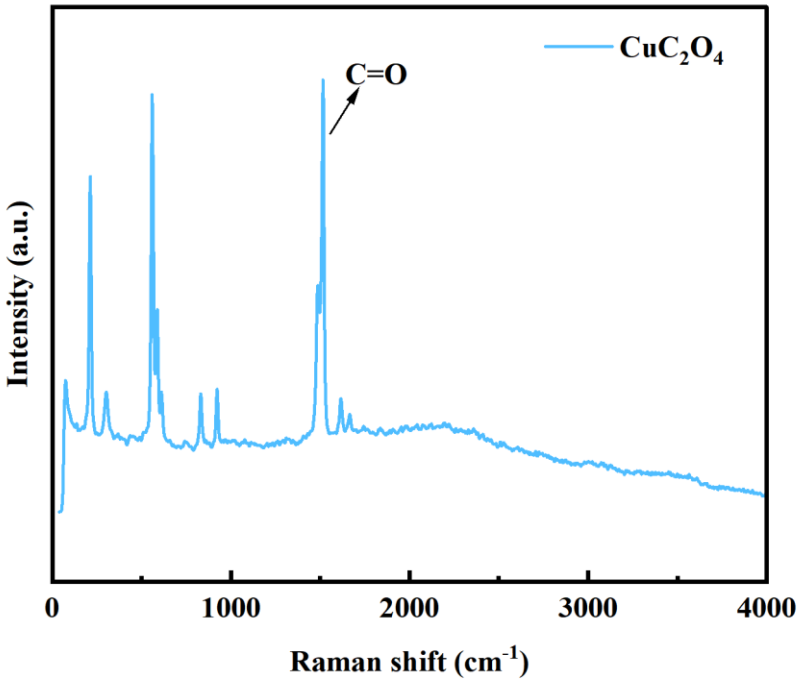
Supplementary Figure 9. Cross-sectional SEM images of the cycled (a) ZP and (b) ZP@CuC_2O_4 electrodes, showing the through-thickness morphology after electrochemical cycling.



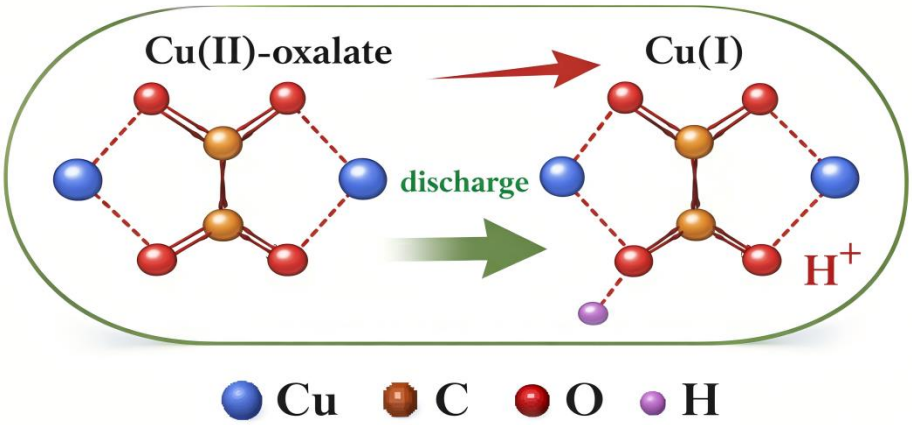
Supplementary Figure 10. Post-cycling SEM images and corresponding EDS elemental mappings of (a–d) ZP and (e–h) ZP@CuC_2O_4 electrodes after cycling at 40 °C.



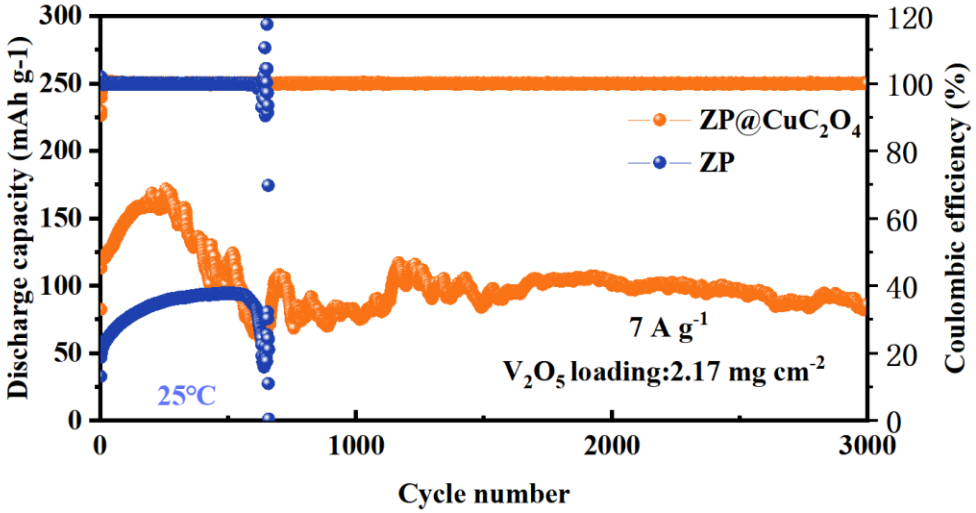
Supplementary Figure 11. XRD pattern of CuC_2O_4 powder.



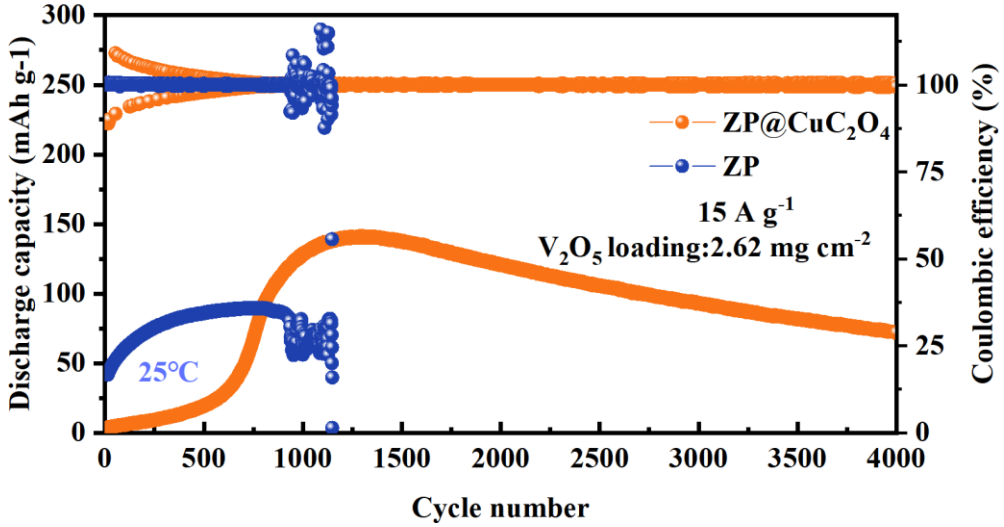
Supplementary Figure 12. Raman spectrum of CuC_2O_4 powder.



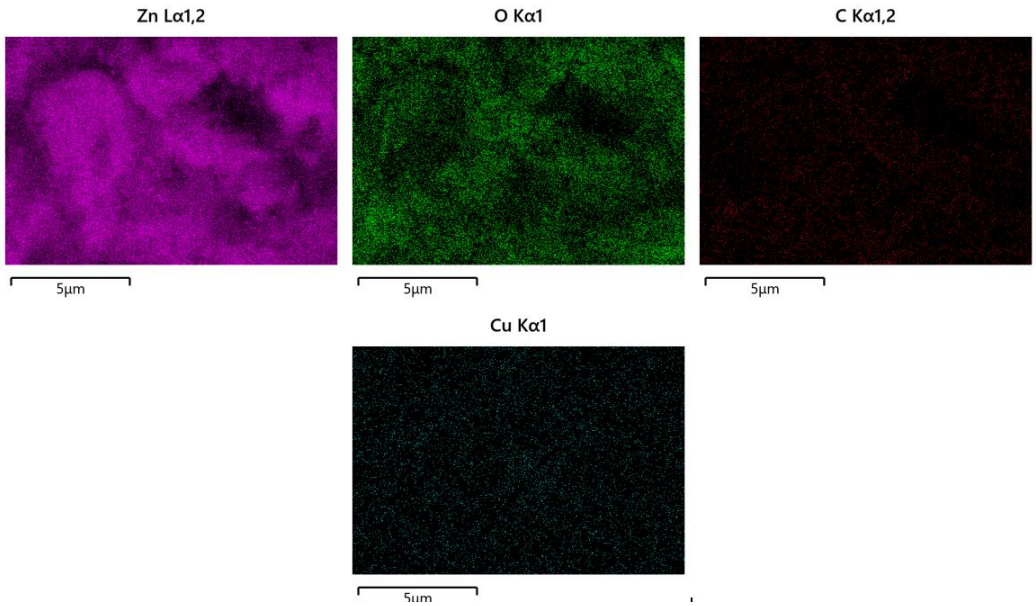
Supplementary Figure 13. Schematic illustration of the discharge-induced structural evolution from Cu(II)-oxalate to a Cu(I)-related coordination environment.



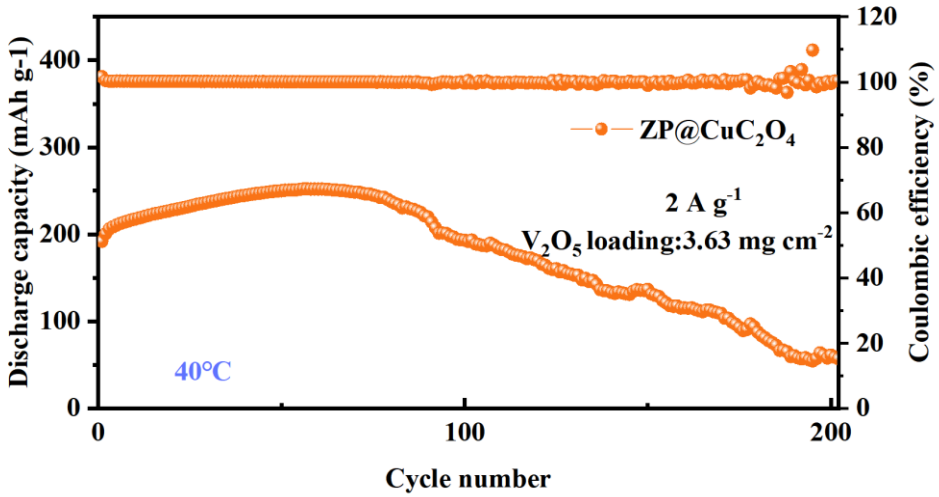
Supplementary Figure 14. Cycling performance and Coulombic efficiency of Zn//V_2O_5 full cells employing ZP and ZP@CuC_2O_4 anodes at 25 °C and 7 A g^{-1}.



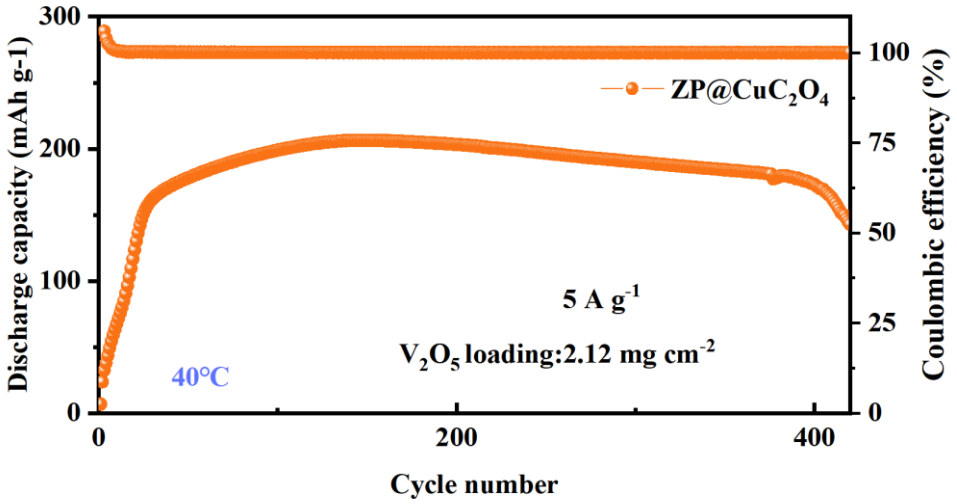
Supplementary Figure 15. Cycling performance and Coulombic efficiency of Zn//V_2O_5 full cells employing ZP and ZP@CuC_2O_4 anodes at 25 °C and 15 A g^{-1}.



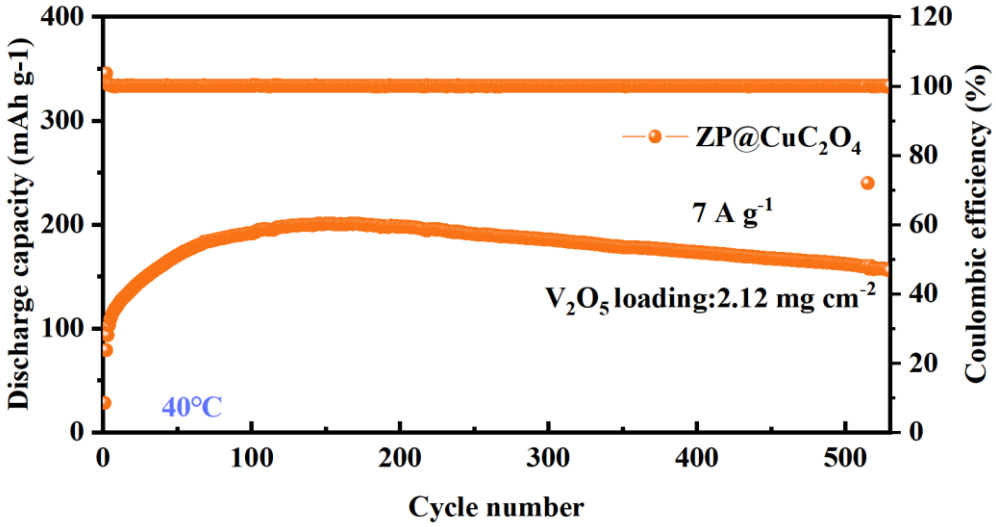
Supplementary Figure 16. Corresponding EDS mapping of the ZP@CuC_2O_4 electrode after 100 cycles in the Zn//V_2O_5 full cell at 5 A g^{-1}.



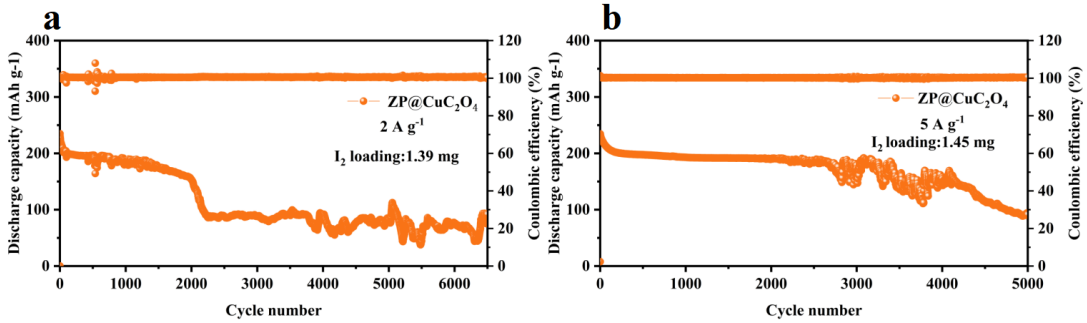
Supplementary Figure 17. Cycling performance and Coulombic efficiency of Zn//V_2O_5 full cells employing ZP@CuC_2O_4 anodes at 40 °C and 2 A g^{-1}.



Supplementary Figure 18. Cycling performance and Coulombic efficiency of Zn//V_2O_5 full cells employing ZP@CuC_2O_4 anodes at 40 °C and 5 A g^{-1}.



Supplementary Figure 19. Cycling performance and Coulombic efficiency of Zn//V_2O_5 full cells employing ZP@CuC_2O_4 anodes at 40 °C and 7 A g^{-1}.



Supplementary Figure 20. Long-term cycling performance and Coulombic efficiency of Zn//I_2 full cells employing the ZP@CuC_2O_4 anode at (a) 2 A g^{-1} with an I_2 loading of 1.39 mg and (b) 5 A g^{-1} with an I_2 loading of 1.45 mg.

Supplementary Table 1. Comparison of cycling lifespans among different reported zinc-based electrode architectures in Zn//Zn symmetric cells

Zinc-based Electrode	Anode type	Current density, Capacity (mA cm^{-2}, mAh cm^{-2})	Lifespan (h)	Ref.
DDA-MXene@Zn-p	Zn powder	0.5-0.5	355	[1]
Zn/rGO	Zn foil	0.4-0.4	300	[2]
ZF@CB-NFC	Zn foil	0.5-0.5	400	[3]
r-Zn	Zn foil	1-0.2	400	[4]
Zn/CNT	3D Zn/CNT host	2-2	200	[5]
Zn@PG	Zn powder	1-1	400	[6]
Zn-PD	Zn powder	1-1	240	[7]
ss-ZnP	Zn powder	1-1	400	[8]
2D-Zn	Zn powder	1-0.5	30	[9]
CuO@Zn	Zn powder	1-0.5	260	[10]
Our work	Zn powder	1-1	706	

Paired values in the "Current density, Capacity" column denote the current density (mA cm^{-2}) followed by the areal capacity (mAh cm^{-2}). For example, "0.5–0.5" represents 0.5 mA cm^{-2} and 0.5 mAh cm^{-2}, while "1–0.2" represents 1 mA cm^{-2} and 0.2 mAh cm^{-2}.

Supplementary Table 2. Corresponding EDS Elemental Mapping Sum Spectrum of the ZP@CuC_2O_4 electrode after 100 cycles in the Zn//V_2O_5 full cell at 5 A g^{-1}

Elemental Mapping Sum Spectrum		
Element	**Line Type**	**wt%**
C	K-series	9.29
O	K-series	11.60
Cu	L-series	1.57
Zn	L-series	77.54
Total		100.00

Supplementary Table 3. Practical parameters of the Zn//V_2O_5 pouch cells shown in Figures 5i and 5j

Parameter	**Figure 5i**	**Figure 5j**
Cathode loading (mg cm^{-2})	5.72	4.68
Zn loading (mg cm^{-2})	≈ 3.92	≈ 3.92
Theoretical Zn areal capacity (mAh cm^{-2})	≈ 3.22	≈ 3.22
N/P capacity ratio	≈ 1.91	≈ 2.33
Zn-anode DOD (%)	≈ 52.4	≈ 42.8
Doctor-blade gap (μm)	100	100
Electrolyte amount (mL)	≈ 5	≈ 5
E/C ratio (μL mAh^{-1})	≈ 119	≈ 145
Initial discharge capacity (mAh g^{-1})	9.508	71.013
Final discharge capacity (mAh g^{-1})	61.330	59.743
Corresponding cycle number	350	1000
Capacity retention (%)	28.7	84.1

For Figure 5i, the cell underwent activation during the first 80 cycles. Capacity retention was calculated by dividing the discharge capacity at cycle 350 by that at cycle 80, selected as the post-activation reference cycle.

REFERENCES

1. Tang, W.; Zhang, L.; Liu, Y.; Wang, S.; Zhang, J. A dual-functional DMDAAC electrode enhancer with hydrophobic effect for highly stable Zn powder composite anode. Energy Storage Mater. 2025, 76, 104127. DOI: 10.1016/j.ensm.2025.104127.

2. Xia, A.; Pu, X.; Tao, Y.; Liu, H.; Wang, Y. Graphene oxide spontaneous reduction and self-assembly on the zinc metal surface enabling a dendrite-free anode for long-life zinc rechargeable aqueous batteries. Appl. Surf. Sci. 2019, 481, 852-859. DOI: 10.1016/j.apsusc.2019.03.197.

3. Wang, A.; Zhou, W.; Huang, A.; et al. Modifying the Zn anode with carbon black coating and nanofibrillated cellulose binder: A strategy to realize dendrite-free Zn-MnO_2 batteries. J. Colloid Interface Sci. 2020, 577, 256-264. DOI: 10.1016/j.jcis.2020.05.102.

4. Guo, N.; Huo, W.; Dong, X.; et al. A review on 3D zinc anodes for zinc ion batteries. Small Methods 2022, 6, 2200597. DOI: 10.1002/smtd.202200597.

5. Zeng, Y.; Zhang, X.; Qin, R.; et al. Dendrite-free zinc deposition induced by multifunctional CNT frameworks for stable flexible Zn-ion batteries. Adv. Mater. 2019, 31, 1903675. DOI: 10.1002/adma.201903675.

6. Du, W.; Huang, S.; Zhang, Y.; Ye, M.; Li, C. C. Enable commercial zinc powders for dendrite-free zinc anode with improved utilization rate by pristine graphene hybridization. Energy Storage Mater. 2022, 45, 465-473. DOI: 10.1016/j.ensm.2021.12.007.

7. Li, Q.; Tang, S.; Luo, R.; et al. Regulating the local chemical environment of Zn powder surface by multi-site anchoring effect to achieve highly stable Zn anode. Energy Storage Mater. 2024, 66, 103229. DOI: 10.1016/j.ensm.2024.103229.

8. Cao, C.; Zhou, K.; Du, W.; et al. Designing soft solid-like viscoelastic zinc powder anode toward high-performance aqueous zinc-ion batteries. Adv. Energy Mater. 2023, 13, 2301835. DOI: 10.1002/aenm.202301835.

9. Cao, P.; Meng, Q.; Li, C.; et al. Dimensionality reduction engineering to construct a highly stable Zn powder anode in aqueous Zn-ion batteries. ACS Appl. Energy Mater. 2024, 7, 479-486. DOI: 10.1021/acsaem.3c02385.

10. Liu, G.-Q.; Fu, B.; Liu, Z.-X.; Li, L.-Y.; Liang, S.-Q.; Fang, G.-Z. Copper oxide-modified highly reversible Zn powder anode for aqueous Zn metal batteries. Rare Met. 2024, 43, 5005-5016. DOI: 10.1007/s12598-024-02869-5.